Struct Chem (2014) 25:1495–1503
DOI 10.1007/s11224-014-0426-2

ORIGINAL RESEARCH

Direct ab initio dynamics calculations of thermal rate constants for the $CH_4 + O_2 = CH_3 + HO_2$ reaction

Tam V.-T. Mai · Minh v. Duong · Xuan T. Le · Lam K. Huynh · Artur Ratkiewicz

Received: 20 January 2014 / Accepted: 12 March 2014 / Published online: 4 April 2014

Abstract Thermal rate constants of the $CH_4 + O_2 = CH_3 + HO_2$ reaction were calculated from *first principles* using both the conventional transition state theory (TST) and canonical variational TST methods with correction from the explicit hindered rotation treatment. The CCSD(T)/aug-cc-pVTZ//BH&HLYP/aug-cc-pVDZ method was used to characterize the necessary potential energy surface along the minimum energy path. We found that the correction for hindered rotation treatment, as well as the re-crossing effects noticeably affect the rate constants of the title process. The calculated rate constants for both forward and reverse directions are expressed in the modified Arrhenius form as $k_{\text{forward}}^{\text{CVT/HR}} = 2.157 \times 10^{-18} \times T^{2.412} \times \exp\left(-\frac{25812}{T}\right)$ and $k_{\text{reverse}}^{\text{CVT/HR}} = 1.375 \times 10^{-19} \times T^{2.183} \times \exp\left(\frac{2032}{T}\right)$ (cm^3 $molecule^{-1}$ s^{-1}) for the temperature range of 300–2,500 K. Being in good agreement with literature data, the results provide solid basis information for the investigation of the entire alkane + O_2 = alkyl radical + HO_2 reaction class.

Keywords Methane oxidation · Hydrogen abstraction · Rate constants · Methyl radical · Hydroperoxy radical

Introduction

Reaction of methane with oxygen, $CH_4 + O_2$, is known to play a significant role in many important industrial processes such as the natural gas combustion process, direct oxidation of methane to methanol, and partial oxidative processes to produce ethylene and ethane [1]. Although the reaction $CH_4 + O_2$ is known to have a high barrier of around 60 kcal mol^{-1} [2], it is important in most of combustion systems due to the abundance of O_2 as in usual combustion environment. For example, it is a crucial reaction in the initiation of methane–oxygen combustion in which the concentration of both methane and oxygen is significant. In such a case, there are no other competing channels due to the low concentration of other radicals or species, and thus this reaction is the sole initiation process [3, 4]. For this reason, reliable thermal rate constants in a wide range of temperature for the reaction $CH_4 + O_2(^3\Sigma) = CH_3 + HO_2$ (Rxn. 1) is of great interest and also of particular importance to modeling of CH_4 oxidation [5].

Determination of reliable thermal rate constants for the reaction between methane and oxygen molecule is rather difficult by experiments due to the interference of secondary reactions of the involved molecules such as methyl and HO_2. For that reason, there is a few numbers of available experimental data for this reaction in limited conditions. Particularly, only upper limit rate constant is determined indirectly at one temperature point of 830 K in the low-pressure range of 0.15–0.56 bar in the O_2 bath gas [6]. More recently, Rxn.1 has received two experimental investigations and that was by Srinivasan et al. [4] for the

Electronic supplementary material The online version of this article (doi:10.1007/s11224-014-0426-2) contains supplementary material, which is available to authorized users.

T. V.-T. Mai · M. v. Duong · X. T. Le · L. K. Huynh (✉)
Institute for Computational Science and Technology,
Ho Chi Minh City, Vietnam
e-mail: hklam@hcmiu.edu.vn; lamhuynh.us@gmail.com

L. K. Huynh
International University, Vietnam National University,
Ho Chi Minh City, Vietnam

A. Ratkiewicz (✉)
Chemistry Institute, University of Bialystok, Hurtowa 1,
15-399 Bialystok, Poland
e-mail: artrat@uwb.edu.pl

forward reaction in 1,655–1,822 K and by Hong et al. [7] for reverse reaction in 1,054–1,249 K. The results of such measurements have some uncertainty due to the above difficulties, especially for the reverse reaction because of the difficulty in measuring the concentrations of both radicals accurately for rate constant determinations. In addition, for kinetic modeling purposes, we are interested in reliable kinetic data in a much larger range of temperature (e.g., 300–2,500 K).

Theoretically, there have been several previous estimations [2, 4, 5, 8–15] on the thermal rate constants for the $CH_4 + O_2$ reaction. Generally, some of these estimations are derived indirectly from complex mechanisms which are frequently based on inadequate experimental/computed data [4, 5, 7–11, 13–15]; while others were estimated from thermodynamic properties [2, 4, 5, 8–15]. In the previous theoretical developments, neither re-crossing effects nor explicit rigorous hindered rotation treatment of some low-frequency motions were accounted for this title reaction [4]. Furthermore, accurate thermal rate constants for the $CH_4 + O_2$ reaction can also be used with our recent reaction class transition state theory (RC-TST) [16–25] to predict all reactions in the entire alkane + O_2 reaction class. The RC-TST is a known reliable method in obtaining good kinetic parameters for numerous elementary reactions in a given class on the fly by extrapolating highly-accurate rate constants of the reference reaction, which is the title reaction in this study, to rate constants of any reaction in the class within the TST framework. For the reasons above, it is important to carry out accurate direct ab initio study to both verify the accuracy of previously reported data and also to provide more reliable kinetic parameters for the title reaction in a wider range of temperature.

In this study, we have performed accurate calculations for the thermal rate constants of the $CH_4 + O_2$ reactions using a direct ab initio dynamics approach with the variational canonical transition state theory (CVT) where potential energy surface information is calculated from an accurate electronic structure theory. The calculated values are compared to the literature data, so that the suggested rate constant can be confidently used in the temperature range of 300–2,500 K.

Computational details

Electronic structure calculations

All the electronic structure calculations were carried out using the program package GAUSSIAN 09 [26]. A hybrid non-local density functional theory (DFT), particularly Becke's half-and-half [27] (BH&H) non-local exchange and Lee–Yang–Parr (LYP) [28] non-local correlation functionals, was employed with the Dunning's correlation-consistent polarized valence double-zeta basis set [3*s*2*p*1*d*/2*s*1*p*] denoted as aug-cc-pVDZ [29] for determining structural and vibrational frequency information. It has been found previously that the BH&HLYP DFT is sufficiently accurate for predicting the properties of reactants, products, as well as transition state, e.g., geometry and frequency, for hydrogen abstraction reactions by a radical species [30–33]. Here, we would like to explore whether it can be effectively used for the case of hydrogen abstraction by neutral molecules. It is done by comparison DFT data with the Quadratic Configuration Interaction with perturbative inclusion of the singles and doubles excitations (QCISD) results, which used to be credited with the higher confidence in the quantitative respect of their ability to properly predict important molecular parameters.

The minimum energy path (MEP) of the potential energy surface is also obtained at BH&HLYP/aug-cc-pVDZ using the intrinsic reaction coordinate theory (IRC) with a gradient step size of 0.1 $(amu)^{1/2}$ bohr. Force constants at 20 selected points along the MEP (10 points in the reactant channel and 10 points in the product channel) were determined to obtain necessary potential energy surface information for CVT calculation. The points were chosen based on the curvature of the MEP and of the geometrical parameters as functions of the reaction coordinate according to our autofocusing technique [34]. Energetic information along the MEP is further refined by using the couple cluster method including single and double substitutions with a quasi-perturbative triples contribution [CCSD(T)] [35] with aug-cc-pVTZ basis set at the BH&HLYP/aug-cc-pVDZ geometry, which is denoted as [CCSD(T)/aug-cc-pVTZ//BHHLYP/aug-cc-pVDZ]. The CCSD(T) energies, accompanied with the BH&HLYP/aug-cc-pVDZ geometries and frequencies, were then used to calculate the rate constants.

Rate constant calculations

The rate constants for this reaction at the two methods, TST and CVT theories, are calculated employing the MWMC code [36], which inherited the Variational TST subroutine of the TheRate code [34], which has been previously validated for its ability to accurate predict rate constants for different reaction classes. In these calculations, overall rotations are treated classically and vibrations are treated using the harmonic approximation except the mode corresponding to the rotation of the $–CH_3$ group, which is treated as the hindered internal rotation using the method implemented in the MWMC code.

In the MWMC program, the hindered internal rotation is explicitly treated in the most accurate manner as described

hereafter. The 1-D Schrödinger equation for a hindered internal rotor (HIR) is given as

$$-\frac{1}{2I_{\text{red}}}\cdot\frac{d^2\Psi_{\text{hir}}}{d\theta^2}+V(\theta)\Psi_{\text{hir}}=E\Psi_{\text{hir}}, \quad (1)$$

where E is the energy; I_{red} is the reduced moment of inertia for the considered rotation and is calculated as $I^{(2,3)}$ according to East and Radom [37] on the basis of the original work by Kilpatrick and Pitzer [38]. The hindrance potential, $V(\theta)$, is directly computed as a function of torsional angle, θ, with a step of 10° Specifically for this system, it was obtained at the BHandHLYP/aug-cc-pVDZ level via relaxed surface scans with the step size of 10° for dihedral angles that correspond to the rotations. In order to solve the HIR equation, we cast it into a Mathieu-type equation by representing the hindrance potential as a Fourier series, $V(\theta)=\sum_{l=-L}^{L}c_l e^{il\theta}$, in which L is some cut-off number depending on the nature of the potential. The wave function was expanded as a harmonic series, $|m\rangle=\frac{1}{\sqrt{2\pi}}e^{im\theta}$, and plugged into HIR equation. The matrix elements for the Hamiltonian are then given by

$$\begin{aligned}H_{mn}&\equiv\langle m|H|n\rangle\\&=\frac{1}{2\pi}\int_0^{2\pi}e^{-im\theta}\left(-\frac{1}{2I_{\text{red}}}\frac{\partial^2}{\partial\theta^2}+\sum_{l=-L}^{L}C_l e^{il\theta}\right)e^{in\theta}\mathrm{d}\theta.\\&=\frac{1}{2I_{\text{red}}}m^2\delta_{mn}+c_{m-n}\end{aligned} \quad (2)$$

The matrix can be diagonalized to obtain its eigenvalue spectrum, which are the energy levels of the considered rotor. These information are used to calculate the partition function and the contributions to the thermodynamic functions. Thermal rate constants are calculated in the temperature range of 300–2,500 K, which is sufficient for combustion applications.

Results and discussion

Potential energy surface

BH&HLYP optimized geometries of the reactants (CH_4 and O_2), products (CH_3 and HO_2), transition state and the intermediate complex in the product channel are shown in Fig. 1. The experimental data available in the literature are also given in parentheses. The BH&HLYP/aug-cc-pVDZ gives a shorter bond length for oxygen molecule with the difference of 0.025 Å when compared to the experimental data, while the calculated C–H bond length in methane and methyl radical (0.001 and 0.002 Å for CH_4 and CH_3, respectively) is a bit larger than experimental value. Compared to the geometries of the reactants and products, it is easily seen that the BH&HLYP gives a product-like transition state because the C1–H4 distance is much larger than C–H bond length in CH_4 (1.492 Å compared to 1.089 Å) and the H4–O6 distance is very close to the O–H bond length in the product OOH (1.089 Å compared to 0.964 Å).

To verify the accuracy of the BH&HLYP level of theory, we compare its results to those obtained with the QCISD method. The QCISD results are also given in Fig. 1. It is seen that the BH&HLYP tends to give shorter bond lengths and angles than the QCISD. For the reactants and products, the geometries at the two levels are almost the same with the maximum bond length difference of 0.043Å at O–O bond in OOH radical. The bond angles are almost identical at both levels, which appear to perform equally well when compared to experimental data. For the transition state, the geometries at the two levels are still very close one to another, except for the bond between two oxygen atoms, where the BH&HLYP calculated bond length is 0.039 Å shorter than that obtained with the QCISD method. Such a difference was also found for the OOH radical. Since the O–O bond is only a spectator in the $CH_4 + O_2$ reaction, we can expect this difference to have only a minor effect on the calculated rate constants.

BH&HLYP harmonic vibrational frequencies for the reactants, products, transitions state, and complex are presented in Supplementary Table S1. In general, both (i.e., BH&HLYP/aug-cc-pVDZ and QCISD/aug-cc-pVDZ) methodologies give similar frequencies for reactants, products, and even for transition state, they are slightly higher than those available in the literature. Note that the use of the scaling frequency factor of 0.9547 for BH&HLYP suggested by Merrick et al. [44] makes the difference smaller.

In comparison with previous electronic structure calculations for this reaction, it is worth mentioning that the geometries of the transition state obtained in this study with the HF (Hartree–Fock), BH&HLYP, QCISD methods are all in the *cis*-configuration. Optimized TS geometries at the HF and CISD(+Q) levels of theory reported by Hamilton and Schaefer [45] are in the *trans*-configuration. The differences in the energetically more favorable TS structure may be due to the differences in the basis sets and levels of theory used in both studies. Note that since the mode for interchange between the two configurations has a rather low frequency of 32 cm^{-1} at the BH&HLYP/aug-cc-pVDZ level, and in the subsequent thermal rate constant calculations, we treated this mode as hindered rotation (as discussed below). Therefore, it is not crucial to distinguish the two different configurations in obtaining accurate rate constants for this reaction.

Energetic information of stationary points along the reaction coordinate is listed in Table 1 and the schematic

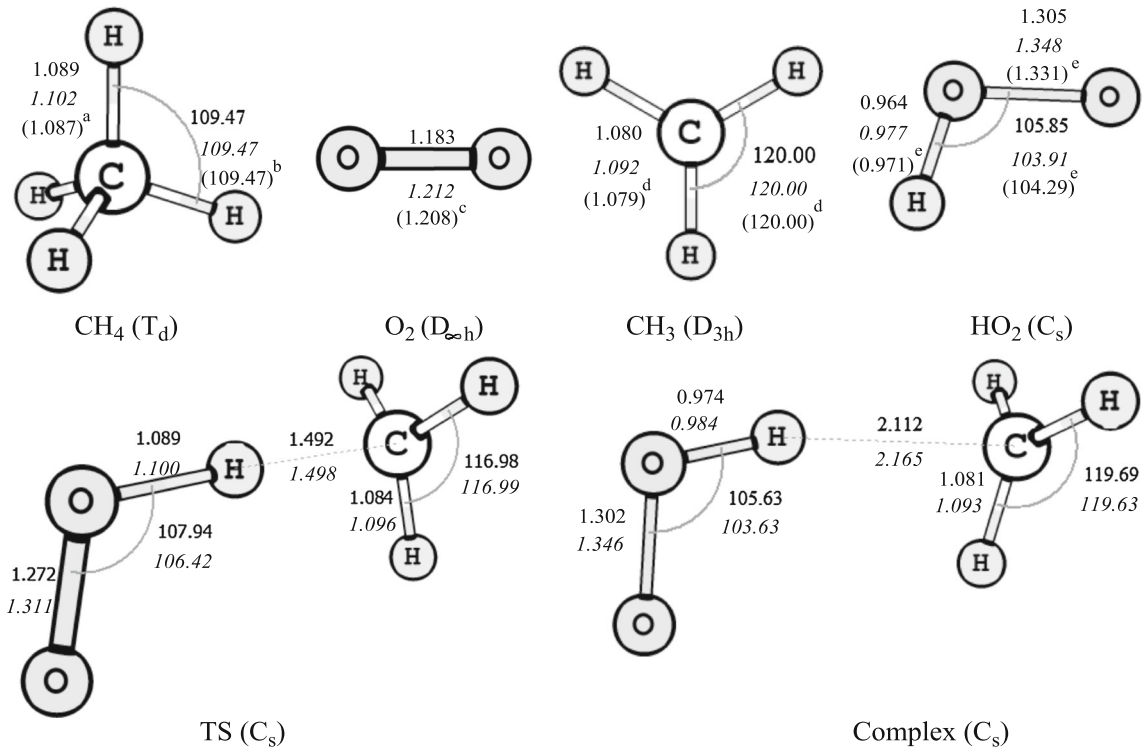

Fig. 1 Optimized geometries (distances in Å and angles in degrees) of the reactants, products, complex, and transition state at the BH&HLYP/aug-cc-pVDZ and QCISD/aug-cc-pVDZ levels (*italic numbers*). The *numbers in the parentheses* are the experimental values from the work of: [a] Hirota et al. [39], [b] Sverdlov et al. [40]; [c] Huber et al. [41]; [d] Herzberg et al. [42] and [e] Lubic et al. [43]

Table 1 The reaction energy and the reaction barrier are also given in kcal mol^{-1}, numbers in parentheses include zero-point energy correction at different levels of theory at 0 K

	CCSD(T)/aug-cc-pVTZ//BHHLYP/aug-cc-pVDZ	QCISD/aug-cc-pVDZ	Literature
Classical barrier	56.2 (52.7)	55.8 (52.3)	56.5[a] (52.9)[a]
Complex binding energy[c]	4.0 (2.6)	3.6 (2.2)	4.0[a] (2.5)[a]
Reaction energy	57.2 (54.6)	55.4 (52.6)	57.6[a] (54.8)[a] (55.4 ± 0.07)[b]

[a] From the work of Srinivasan et al. [4]

[b] From the work of Ruscic [46]

[c] Binding energy = E(CH_3 + HO_2) - E(complex)

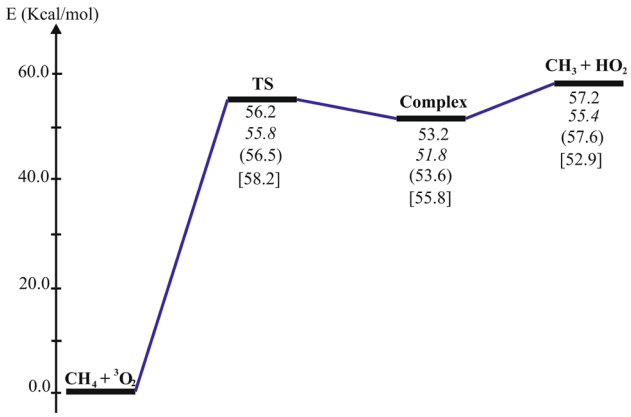

Fig. 2 Schematic energy profile (0 K) of the reaction $CH_4 + O_2$ at CCSD(T)/aug-cc-pVTZ//BHandHLYP/aug-cc-pVDZ and QCISD/aug-cc-pVDZ levels (*italic numbers*), *numbers in parentheses* were derived from Srinivasan et al. [4] at 0 K and *numbers in square parentheses* are the Gibbs free energy at 298 K. All values are in kcal mol^{-1}

energy profile is shown in Fig. 2. The most accurate energetic results from this study are those from single-point energy CCSD(T)/aug-cc-pVTZ calculations at the optimized BH&HLYP/aug-cc-pVTZ geometries. The CH_4 + O_2 reaction is endothermic with the reaction energy of 57.2 kcal mol^{-1}. The calculated classical barrier for this reaction is 56.2 kcal mol^{-1} which is 1.0 kcal mol^{-1} below the existing channel. The zero-point corrected barrier is still lower than the reaction energy (e.g., 52.7 and 54.6, respectively). These results are in good agreement with data of Srinivasan et al. [4] and Ruscic et al. [46].

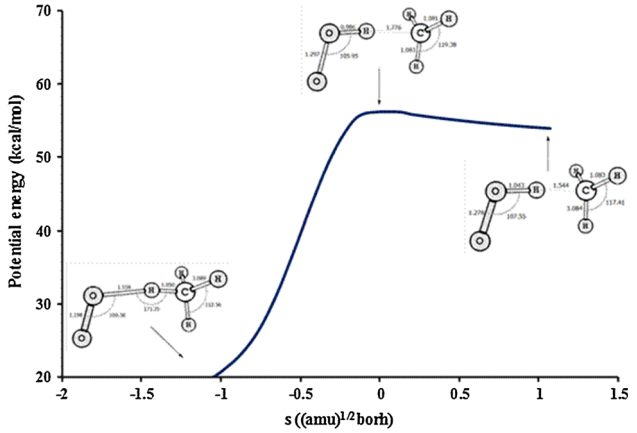

Fig. 3 Representative part of energy profile along the IRC with a step size of 0.1 $(amu)^{1/2}$borh for $CH_4 + {}^3O_2 \rightarrow CH_3\cdots HO_2$ (complex) at CCSD(T)/aug-cc-pVTZ//BHandHLYP/aug-cc-pVDZ level of theory

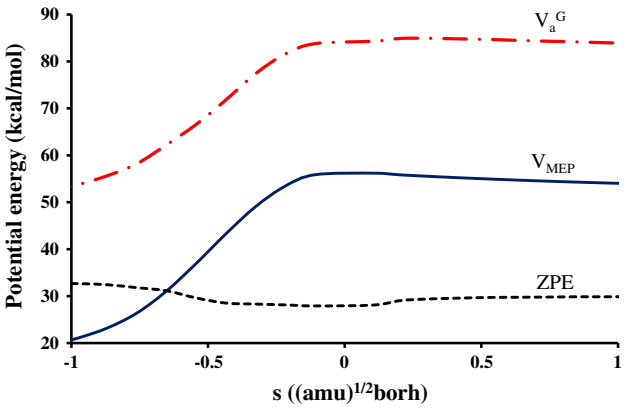

Fig. 4 The classical potential energy (V_{MEP}) total zero-point energy (ZPE) and adiabatic vibrational ground-state potential energy (V_a^G) along the reaction co-ordinate s calculated at CCSD(T)/aug-cc-pVTZ//BHandHLYP/aug-cc-pVDZ level of theory at 0 K. The reference value is the classical energy of the reactants

The weak binding complex in the reaction channel is only 4.0 kcal mol^{-1} below the dissociative products. Interestingly, at higher temperature, the free-energy difference changes the sign (from -3.6 kcal mol^{-1} at 0 K to $+2.9$ kcal mol^{-1} at 298 K) and the free energy of the TS is highest (58.2 kcal/mol at 298 K). Due to its high barrier, the reaction would occur at rather high temperatures, one can expect that if the trajectory has sufficient energy to cross over the dynamical bottleneck, i.e., the maximum of the free energy curve along the reaction coordinate within the CVT formalism is not trapped in this shallow well, at least at the conditions considered in this study. Consequently, the intermediate complex does not play a significant role in the kinetics of the title reaction, thus, we can reasonably assume that the dynamical bottleneck is in the vicinity of the transition state. Such an assumption was previously proven to be valid for the $H_2CO + O_2 \rightarrow HCO + HO_2$ reaction with very similar PES to the title process [47]. It is interesting to note that the QCISD method at the smaller aug-cc-pVDZ basis set predict very similar results to those of CCSD(T)/aug-cc-pVTZ level.

Figure 3 shows the classical energetic profile V_{MEP} (ZPE correction is not included) along the intrinsic reaction coordinate (IRC) connecting the reactants ($CH_4 + O_2$) and the complex ($CH_3\cdots HO_2$) at BH&HLYP/aug-cc-pVDZ level. The reaction coordinate s is defined as the distance along the minimum energy path in the mass-weighted Cartesian coordinate with the origin at the transition state. The initial profile involves the O6–H4 bond formation and H4–C1 bond rupture to form the transition state at $s = 0.0$ $(amu)^{1/2}$borh. This IRC profile together with the molecular information along the MEP is then used for CVT calculations.

Figure 4 shows the classical potential energy V_{MEP}, total zero-point energy, and adiabatic vibrational ground-state potential energy V_a^G along the reaction coordinate. It is important to recall that the potential energy curve is calculated at the CCSD(T)//BH&HLYP level, whereas the

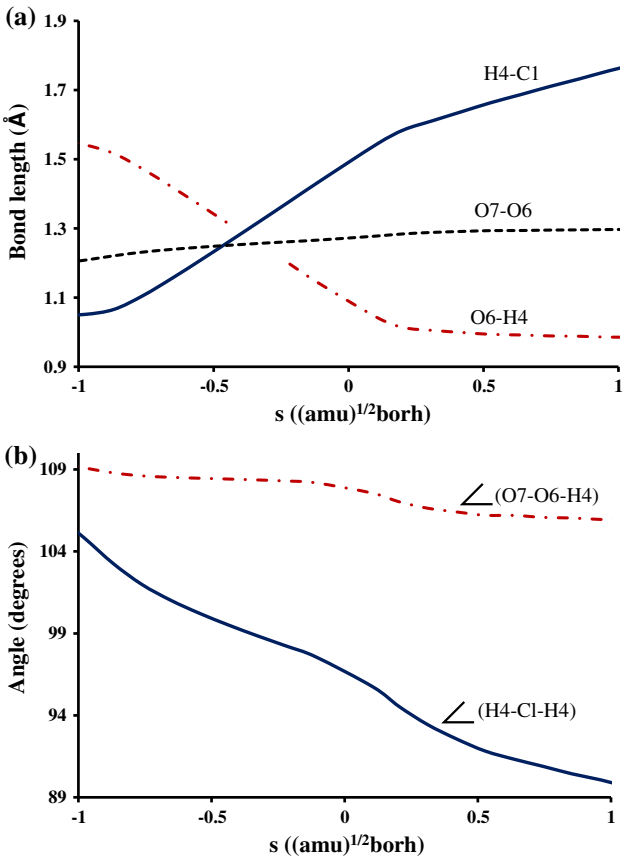

Fig. 5 **a** The changes of H4–C1, O6–H4, and O7–O6 bond lengths and **b** the changes of ∠(H4–C1–H5) and ∠(O7–O6–H4) angles along the reaction coordinate at BH&HLYP/aug-cc-pVDZ level of theory

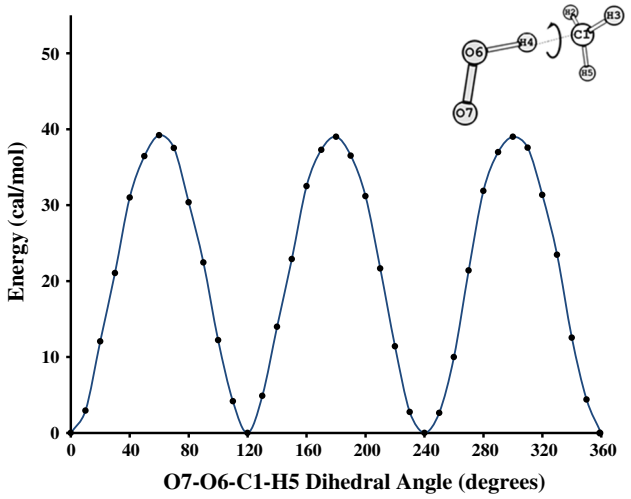

Fig. 6 Hindrance potential of the CH_3 rotation along the O6–C1 axis at the transition state from BH&HLYP/aug-cc-pVDZ calculation

frequencies along the MEP were calculated at the BH&HLYP level. Since the total zero-point energy remains fairly constant along the reaction coordinate, the $V_{MEP}(s)$ and $V_a^G(s)$ curves are similar, and thus the zero-point energy corrected barrier is lower than the classical barrier by about 1.0 kcal mol^{-1}.

The changes of bond lengths along the MEP are plotted in Fig. 5. It is easily seen that the most critical geometry change along the MEP is the active bond lengths H4–C1 and O6–H4. The O7–O6 bond distance remains rather constant along the reaction coordinate as expected of a spectator bond. As the reaction proceeds, the active H4–C1 (breaking) and O6–H4 (forming) bonds lengths change very rapidly in the range of $s = -1.0$ to $s = 0.3$ $(amu)^{1/2}$ bohr. To take a deeper look into this issue, the frequency changes along the MEP over the same reaction region were also plotted in Fig. 4. The mode shown by the solid line, which relates to the breaking H4–C1 bond in the reactant region and the forming O6–H4 bond in the product region, changes sharply in the region from $s = -1.0$ to $s = 0.3$ $(amu)^{1/2}$bohr.

At the transition state, the $–CH_3$ group can internally rotate along the O–C axis; thus the corresponding vibrational mode should be treated as a hindered rotation as discussed previously. Figure 6 presents the hindrance potential which is used to determine the barrier to rotation, the rotational symmetry and the number of rotational minima. The potential is compiled as a relaxed scan with a resolution of 10° at the BH&HLYP/aug-cc-pVDZ level of theory. The effect of treating O–C internal rotation as a hindered rotor is examined later in the rate constants part. This hindrance potential has 3 symmetric minima with a small barrier of 0.04 kcal mol^{-1}.

Rate constants

Due to the relatively flat shape of the V_{MEP} curve in the transition state region (cf. Fig. 3), the high forward barrier (58.2 kcal mol^{-1} at 298 K) and the low reverse barrier (2.4 kcal mol^{-1} at 298 K), we can expect tunneling contribution to be small. Using small curvature tunneling (SCT) method, the calculated tunneling correction factor to the rate constants is close to unity even at 298 K. At higher temperature, the contribution is smaller. This confirms the insignificance of the tunneling contribution.

The rate constants calculated with the TST and CVT methods in the temperature range of 300–2,500 K are given in Table 2. The ratios between the rate constants k^{CVT}/k^{TST} illustrate the magnitude of the re-crossing effect. It can be seen that this ratio decreases as the temperature increases; thus the re-crossing effect is more important at high temperatures as expected. At the room temperature, it accounts for only about 1 % of the total rate. However, at 1,000 K re-crossing effect lowers the rate by 40 %. As mentioned earlier, internal rotational motion of the methyl group is treated as a hindered rotor. It can be seen that the hindered rotation correction factor to the rate constant decreases as the temperature increases. For instance, at the room temperature, it increases the rate constant by a factor of 2.17 at 300 K but decreases by a factor of 0.61 at 1000 K. The Arrhenius expressions for the rate constants calculated at CVT method including the correction from hindered rotation treatment are given below:

$$k_{\text{forward}}^{\text{CVT/HR}} = 2.157 \times 10^{-18} \times T^{2.412} \times \exp\left(-\frac{25812}{T}\right) \quad (3)$$

and

$$k_{reverse}^{CVT/HR} = 1.375 \times 10^{-19} \times T^{2.183} \times \exp\left(\frac{2032}{T}\right), \quad (4)$$

cm^3 $molecule^{-1}$ s^{-1} for the temperature range of 300–2,500 K.

With the inclusion of the hindered internal rotation in the rate constant expression, the Arrhenius parameters A, n, and E_a can be considered as fitting coefficients. To better understand the contribution of the hindered internal rotation, we factored out the rate-constant expression in Eq. (1) into two components: $k(T) = k^{Arrh} \times k^{HR}$, where k^{Arrh} is the rate-constant expression without HR and k^{HR} is the contribution due to the HR of the CH_3 group. The two expressions are given as

$$k^{Arrh} = 1.844 \times 10^{-19} \times T^{2.841} \times \exp\left(\frac{-25803}{T}\right) \quad (5)$$

and

$$k^{HR} = 140.218 \times T^{0.5433} \times \exp\left(\frac{58}{T}\right) \quad (6)$$

Table 2 Calculated TST, CVT rate constants (cm^3 $molecule^{-1}$ s^{-1}) and hindered rotation correction factor for the forward and reverse reaction of $CH_4 + O_2$

Temp (*K*)	k^{TST}	k^{CVT}/k^{TST}	HR factor[a]	$k^{CVT/HR}$	$k^{sug\ b}$
$CH_4 + {}^3O_2 \rightarrow CH_3 + HO_2$					
300	4.10×10^{-50}	0.99	2.17	8.81×10^{-50}	4.26×10^{-50}
400	2.40×10^{-40}	0.88	1.83	3.87×10^{-40}	2.49×10^{-40}
500	2.10×10^{-34}	0.80	1.57	2.64×10^{-34}	2.08×10^{-34}
600	2.10×10^{-30}	0.74	1.43	2.22×10^{-30}	2.02×10^{-30}
700	1.70×10^{-27}	0.69	1.29	1.52×10^{-27}	1.52×10^{-27}
800	2.70×10^{-25}	0.65	1.19	2.08×10^{-25}	2.29×10^{-25}
900	1.50×10^{-23}	0.62	1.07	9.92×10^{-24}	1.18×10^{-23}
1,000	3.70×10^{-22}	0.59	1.03	2.24×10^{-22}	2.84×10^{-22}
1,500	8.30×10^{-18}	0.50	0.81	3.35×10^{-18}	5.09×10^{-18}
2,000	1.60×10^{-15}	0.44	0.69	4.84×10^{-16}	8.59×10^{-16}
2,500	4.40×10^{-14}	0.40	0.61	1.08×10^{-14}	2.14×10^{-14}
$CH_3 + HO_2 \rightarrow CH_4 + {}^3O_2$					
300	1.30×10^{-11}	0.99	2.17	2.79×10^{-11}	1.04×10^{-11}
400	6.90×10^{-12}	0.88	1.83	1.11×10^{-11}	5.55×10^{-12}
500	5.20×10^{-12}	0.80	1.57	6.54×10^{-12}	4.26×10^{-12}
600	4.60×10^{-12}	0.74	1.43	4.86×10^{-12}	3.86×10^{-12}
700	4.60×10^{-12}	0.69	1.29	4.11×10^{-12}	3.78×10^{-12}
800	4.90×10^{-12}	0.65	1.19	3.77×10^{-12}	3.88×10^{-12}
900	5.30×10^{-12}	0.62	1.07	3.51×10^{-12}	4.09×10^{-12}
1,000	5.90×10^{-12}	0.59	1.03	3.58×10^{-12}	4.36×10^{-12}
1,500	1.10×10^{-11}	0.50	0.81	4.44×10^{-12}	6.49×10^{-12}
2,000	2.00×10^{-11}	0.44	0.69	6.05×10^{-12}	9.56×10^{-12}
2,500	3.40×10^{-11}	0.40	0.61	8.35×10^{-12}	1.35×10^{-11}

[a] Correction factor to the rate constant due to the hindered rotation treatment of the methyl internal rotation motion

[b] Suggested values by Srinivasan et al. [4]

[c] Suggested values by Jasper et al. [5]

in cm^3 $molecule^{-1}$ s^{-1} for the temperature range of 300–2,500 K. Within the framework of the Arrhenius expression, $k(T) = A \times T^n \times \exp\left(-E_a/RT\right)$, the value of −58 in Eq. (4) may be considered as the constant E_a^{HR}/R which characterizes "the effective activation energy" for the hindered internal rotation. The small and negative E_a^{HR}/R value suggests that the hindered CH_3 rotor can be considered as a "free-rotor" in the considered temperature range. This value, in fact, is consistent with the very small hindrance barrier of 0.04 kcal mol^{-1} at 0 K for the rotation of CH_3 group along the O6–C1 axis as seen in Fig. 6.

Compared to the latest values of the rate constants available in the literature (also given in Table 2), the results show an excellent agreement. For a more complete comparison, the CVT/HR rate constants and available rate constants in the literature are plotted in Fig. 7. It can be seen that the CVT/HR calculated rate constants are within the uncertainty of the available data over the wide range of temperature 300–2,500 K. Thus, our findings both confirm the accuracy of previously available data and also provide solid basis to extend these to the entire alkane + O_2 → -alkyl radical + ·OOH reaction class, which is vital for quantitative understanding of the combustion of realistic fuels.

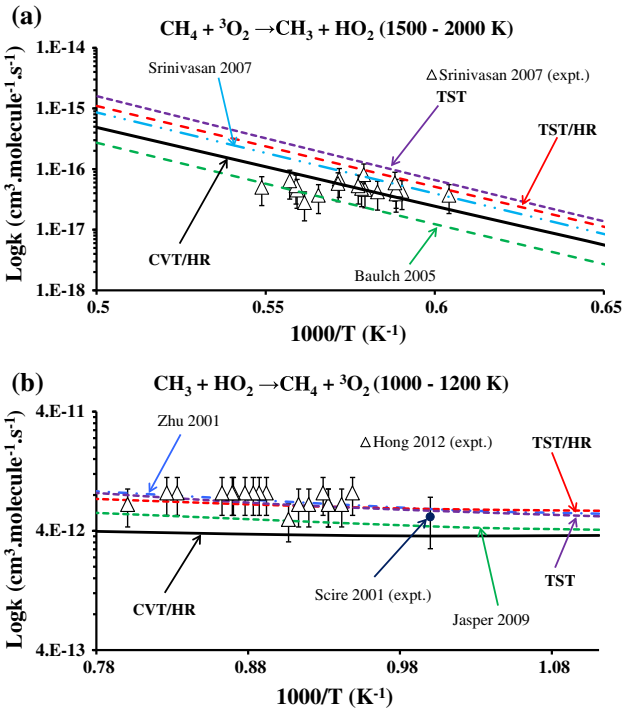

Fig. 7 Comparison of calculated rate constants for (a) $CH_4 + {}^3O_2 \rightarrow CH_3 + HO_2$ and (b) $CH_3 + HO_2 \rightarrow CH_4 + {}^3O_2$ with available data in the literature: Zhu and Lin [13]; Scire et al. [48]; Baulch et al. [15]; Srinivasan et al. [4]; Jasper et al. [5] and Hong et al. [7]

Conclusions

In this paper, the hydrogen abstraction reaction $CH_4 + \cdot O_2 = CH_3 + HO_2$ is studied by a direct ab initio dynamics method based on the variational canonical transition state theory. The potential energy information was calculated from sufficiently accurately level of theory. In particular, structural and frequency information along the reaction coordinate were calculated at the BH&HLYP/aug-cc-pVDZ level, which was shown to have similar level of accuracy as of the QCISD level for these properties. Potential energy along the reaction coordinate was calculated at the CCSD(T)/aug-cc-pVTZ//BH&HLYP/aug-cc-pVDZ level. We found that both re-crossing and hindered rotation effects should be included in the rate constant calculations. The calculated rate constants compare well with those available in the literature, and thus it is suggested to be used for detailed modeling of oxidation of methane and related higher alkanes.

Acknowledgments We thank to the Institute for Computational Science and Technology for computer time and facilities. This research was funded by the Department of Science and Technology at HCMC (administrated by Institute for Computational Science and Technology). We also would like to thank the computational center of the University of Warsaw (ICM) for providing access to the supercomputer resources and the GAUSSIAN 09 program (Grant G33-03).

References

1. Haggin J (1993) Chem Eng News 71(22):23–27
2. Yamaguchi Y, Teng Y, Shimomura S, Tabata K, Suzuki E (1999) J Phys Chem A 103(41):8272–8278
3. Walker RW (1975) Specialist periodical reports: reaction kinetics, chap. 4, vol 1. Burlington House, London, pp 161–211
4. Srinivasan NK, Michael JV, Harding LB, Klippenstein SJ (2007) Combust Flame 149(1–2):104–111
5. Jasper AW, Klippenstein SJ, Harding LB (2009) Proc Combust Inst 32(1):279–286
6. Falconer WE, Knox JH, Trotman-Dickenson AF (1961) J Chem Soc 1961:782–791
7. Hong Z, Davidson DF, Lam K-Y, Hanson RK (2012) Combust Flame 159(10):3007–3013
8. Baulch DL, Cobos CJ, Cox RA, Esscer C, Frank P, Just T, Kerr JA, Pilling MJ, Troe J, Walker RW, Warnatz J (1992) J Phys Chem Ref Data 21:411–429
9. Tsang W, Hampson RF (1986) J Phys Chem Ref Data 15(3):1087–1279
10. Shaw R (1978) J Phys Chem Ref Data 7(3):1179–1190
11. Skinner GB, Lifshitz A, Scheller K, Burcat A (1972) J Chem Phys 56(8):3853–3861
12. Mayer SW, Schieler L (1968) J Phys Chem 72(7):2628–2631
13. Zhu R, Lin MC (2001) J Phys Chem A 105(25):6243–6248
14. Baulch DL, Cobos CJ, Cox RA, Esser C, Frank P, Just T, Kerr JA, Pilling MJ, Troe J, Walker RW, Warnatz J (1992) J Phys Chem Ref Data 21(3):411–736
15. Baulch DL, Bowman CT, Cobos CJ, Cox RA, Just T, Kerr JA, Pilling MJ, Stocker D, Troe J, Tsang W, Walker RW, Warnatz J (2005) J Phys Chem Ref Data 34(3):757–1398
16. Huynh LK, Zhang S, Truong TN (2008) Combust Flame 152(1–2):177–185
17. Kungwan N, Truong TN (2005) J Phys Chem A 109:7742–7750
18. Bankiewicz B, Huynh LK, Ratkiewicz A, Truong TN (2009) J Phys Chem A 113(8):1564–1573
19. Huynh LK, Barriger K, Violi A (2008) J Phys Chem A 112(7):1436–1444
20. Huynh LK, Panasewicz S, Ratkiewicz A, Truong TN (2007) J Phys Chem A 111(11):2156–2165
21. Huynh LK, Ratkiewicz A, Truong TN (2006) J Phys Chem A 110(2):473–484
22. Muszynska M, Ratkiewicz A, Huynh LK, Truong TN (2009) J Phys Chem A 113(29):8327–8336
23. Huynh LK, Truong TN (2008) Theor Chem Acc 120(1–3):107–118
24. Truong TN (2000) J Chem Phys 113(12):4957–4964
25. Zhang S, Truong TN (2003) J Phys Chem A 107(8):1138–1147
26. Frisch MJ, Trucks GW, Schlegel HB, Scuseria GE, Robb MA, Cheeseman JR, Scalmani G, Barone V, Mennucci B, Petersson GA, Nakatsuji H, Caricato M, Li X, Hratchian HP, Izmaylov AF, Bloino J, Zheng G, Sonnenberg JL, Hada M, Ehara M, Toyota K, Fukuda R, Hasegawa J, Ishida M, Nakajima T, Honda Y, Kitao O, Nakai H, Vreven T, J. A. Montgomery J, Peralta JE, Ogliaro F, Bearpark M, Heyd JJ, Brothers E, Kudin KN, Staroverov VN, Kobayashi R, Normand J, Raghavachari K, Rendell A, Burant JC, Iyengar SS, Tomasi J, Cossi M, Rega N, Millam JM, Klene M, Knox JE, Cross JB, Bakken V, Adamo C, Jaramillo J, Gomperts R, Stratmann RE, Yazyev O, Austin AJ, Cammi R, Pomelli C, Ochterski JW, Martin RL, Morokuma K, Zakrzewski VG, Voth GA, Salvador P, Dannenberg JJ, Dapprich S, Daniels AD, Farkas Ö, Foresman JB, Ortiz JV, Cioslowski J, Fox DJ (2009) Gaussian 09, Revision A.1. Gaussian, Inc., Wallingford
27. Becke AD (1993) J Chem Phys 98(2):1372–1377
28. Lee C, Yang W, Parr RG (1988) Phys Rev B 37(2):785–789
29. Dunning TH (1989) J Chem Phys 90(2):1007–1023
30. Truong TN, Duncan W (1994) J Chem Phys 101(9):7408–7414
31. Truong TN, Duncan WT, Tirtowidjojo M (1999) PCCP 1(6):1061–1065
32. Lynch BJ, Fast PL, Harris M, Truhlar DG (2000) J Phys Chem A 104(21):4811–4815
33. Zhang Q, Bell R, Truong TN (1995) J Phys Chem 99(2):592–599
34. Duncan WT, Bell RL, Truong TN (1998) J Comput Chem 19(9):1039–1052
35. Pople JA, Head-Gordon M, Raghavachari K (1987) J Chem Phys 87(10):5968
36. Duong Mv, Huynh LK, Le T, Truong N, Zhang S, Truong TN MultiWell-MultiChannel program suite, Version 2014. https://sites.google.com/site/multiwellmultichannel/
37. East ALL, Radom L (1997) J Chem Phys 106(16):6655–6674
38. Kilpatrick JE, Pitzer KS (1949) J Chem Phys 28:1064–1075
39. Hirota E (1979) J Mol Spectrosc 77(2):213–221
40. Sverdlov LM, Kovner MA, Krainov EP (1974) Vibrational spectra of polyatomic molecules. Wiley, New York
41. Huber KP, Herzberg G (1979) Molecular spectra and molecular Structure. Van Nostrand Reinhold Company, New York
42. Herzberg G (1966) Electronic spectra and electronic structure of polyatomic molecules. Van Nostrand, New York
43. Lubic KG, Amano T, Uehara H, Kawaguchi K, Hirota E (1984) J Chem Phys 81(11):4826–4831

44. Merrick JP, Moran D, Radom L (2007) J Phys Chem A 111(45):11683–11700
45. Hamilton TP, Schaefer HF (1989) J Chem Phys 90(11):6391–6394
46. Ruscic B, Pinzon RE, Laszewski Gv, Kodeboyina D, Burcat A, Leahy D, Montoya D, Wagner AF (2005) J Phys: Conf Ser 16:561–570
47. Huynh LK, Tirtowidjojo M, Truong TN (2009) Chem Phys Lett 469(1–3):81–84
48. Scire JJ, Yetter RA, Dryer FL (2001) Int J Chem Kinet 33(2):75–100